

Experimental Investigation of Flow and Coherent Properties of Excited Non-Circular Liquid Jets

M. Babayan^{1†}, P. Tabatabaee-Hosseini¹, N. Esmaeilzadeh Kandjani¹, S. A. Tafrishi², M. Jafari¹,
and E. Esmaeilzadeh^{1,3†}

¹ Mechanical Engineering Department, University of Tabriz, Tabriz, Iran

² Control Engineering Lab, Mechanical Engineering Department, Kyushu University, Fukuoka, Japan

³ Mechanical Engineering Department, Islamic Azad University, Tabriz Branch, Tabriz, Iran

†Corresponding Author Email: esmazadeh@tabrizu.ac.ir, morsal.babaian@gmail.com

(Received July 24, 2018; accepted December 25, 2018)

ABSTRACT

Non-circular jet is identified as an efficient passive flow-control technique that attracts many research topics. The existence of twine-vortexes is the main reason for dissimilarity between circular and non-circular jets. Which also influences the production of droplets and satellites as well as the jet instability. This investigation presents instability analysis of liquid-gas interface as an applicable conception in free-jet flows. We experiment different jet geometries within a gas ambient in order to study their hydrodynamic behavior. These studies give an appropriate perception about contributing forces that play essential roles in fluid instability. We focus on varying viscosity and surface tension as our excitation techniques. These methods are vital to examine the key properties of non-circular jets such as breakup and decay length, axis-switching wavelength as well as produced droplets and satellites characteristics. First, instabilities of charged liquid jets are investigated by considering the interaction between electric and inertial forces. Also, the viscosity effect was studied for its interaction with the inertial and surface tension forces. In each case, liquid jet in-stability for various nozzle geometries over a specific range of jet velocity is examined. The obtained results illustrate that the geometry of nozzle has an important effect on jet instability. In addition, by increment of We number, the breakup and decay length as well as the axis-switching wavelength are raising. However, by the rise of twin-vortex number, the breakup length increases but the decay length and axis-switching wavelength decrease.

Keywords: Non-circular Free jet; Liquid-gas instability; Axis-switching; Breakup length; Penetration length.

1. INTRODUCTION

Fluid science has provided uncountable excellences in manufacturing and science. However, developing our knowledge about fundamental jet behavior would help to create new branches in this field. Non-circular jets are identified as an efficient method of passive flow control that improves the performance of various practical systems significantly. That also comes with relatively low cost where jet performance relies solely on changes in nozzle geometry.

Jet stability and hydrodynamical parameters of fluid are influenced directly by the nozzle cross-section geometry. Non-circular nozzle shapes have different effects on instabilities of jet interface in comparison to the circular one. They can be applied in the process of mixing subsonic and supersonic jets [Gutmark et al. \(1990\)](#), [Wlezien and Kibens \(1988\)](#), [Tam and Burton \(1984\)](#). They also increase the efficiency of combustion engines by decreasing breakup length of

the jet which converts fuel into minuscule droplets and raises the chemical reactions [Gutmark et al. \(1989\)](#). From the heat transfer point of view, instabilities on the jet surface besides changing the flow patterns will also enhance the heat transfer [Ho and Gutmark \(1987\)](#). Light metal powders can be manufactured by cooling dielectric liquids, where formation of the particles requires precise studies on jet instabilities under the effect of lateral electrical field [Kandjani et al. \(2010\)](#), [Khoshnevis et al. \(2014\)](#). Another remarkable application of jet flow is spray drift of pesticides in the agricultural field [Nuyttens et al. \(2010\)](#), [Nuyttens et al. \(2006\)](#).

The flow patterns associated with non-circular jets include vortex evolution and interaction mechanisms, as well as flow instabilities and fine-scale turbulence augmentation. Also, a general nozzle geometry comparison for elliptical, triangular and quadrangular cross-sections has been analyzed by different researches [Reeder and Samimy \(1996\)](#), [Baty and Morris \(1995\)](#). One of the earliest stud-ies

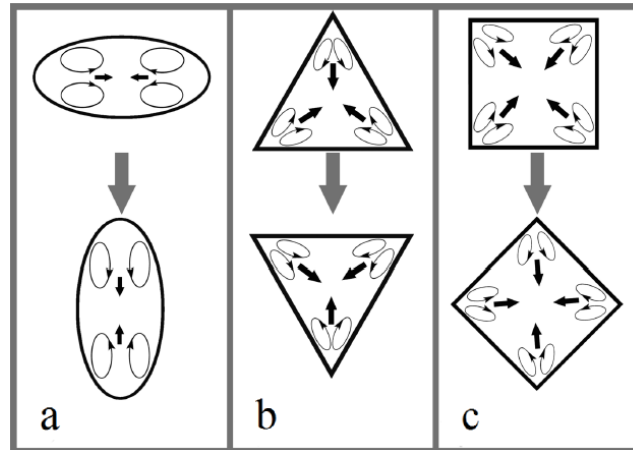


Fig. 1. Twin-vortex motions in corners or segments with greater curvatures leading to axis-switching phenomenon; a) elliptical, b) triangular and c) quadrangular jets.

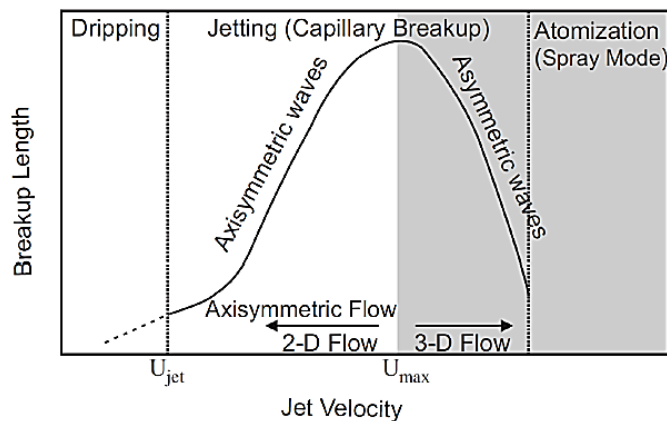


Fig. 2. Different breakup modes of jet column in silent medium [Kitamura *et al.* \(1982\)](#).

on non-circular jet stability and their application to manipulate jet-mixing behavior was carried out by [Crighton \(1973\)](#). [Rayleigh \(1879\)](#) as a pioneer gave a theoretical description for non-circular jets. He studied a cylinder of incompressible in-viscid liquid with an undulating jet cross section which had infinitesimal amplitudes. Recently, [Rajesh *et al.* \(2016\)](#) has presented an experimental study on the wavelength and oscillation amplitude of non-circular jets discharging from elliptical, triangular and square nozzles.

Considering Fig. 1, the main difference between non-circular jet instabilities and circular one is in the existence of twin-vortices in corners of triangular and quadrangular jets, and also in segments of maximum curvatures in the elliptical jet. Twin-vortex numbers are zero, two, three and four in circle, elliptic, triangle and quadrangle jets respectively. Mentioned vortices had been perceived experimentally by flow visualization, [Reeder and Samimy \(1996\)](#), [Zaman *et al.* \(1994\)](#). These twin-vortices change the geometry of liquid-gas interface. Subsequently, contraction and expansion of the interface will be in the central axis of the jet in contrast to the circular one. For the case of the elliptical nozzle, it is easy to observe the twin-

vortices since it is two dimensional. On the other hand, for the other cases with corners, effects of vortices are three-dimensional that cannot be easily detected. Axis-switching occurs at the beginning – limited length – of the jet and then gradually turns to normal waves.

Stability theory shows the effects of initial momentum, aspect ratio and radius of curvature on the initial flow evolution. For example, the sensitivity of elliptic jets towards the distribution and relevant momentum thickness is observed in [Schadow *et al.* \(1987\)](#), [Quinn \(1989\)](#), and [Lee and Baek \(1994\)](#). It was discovered that the occurrence of axis-switching, its locations and entrainment rates change by different aspect ratios of elliptical jets.

In recent years, different scholars have studied elliptical liquid jets in order to understand the jet instability and breakup behavior at different operational conditions [Kasyap *et al.* \(2008\)](#), [Amini and Dolatabadi \(2011\)](#), [Amini *et al.* \(2014\)](#), [Muthukumar and Vaidyanathan \(2014\)](#), [Sharma and Fang \(2014\)](#), [Sharma and Fang \(2015\)](#), [Wang and Fang \(2015\)](#). Different jet breakup modes are depicted in Fig. 2 where break up length is plotted versus jet velocity. For low velocities, continues flow

of jet is not formed, and droplets are constructed instantaneously on nozzle's outlet which is called dripping mode. As the velocity increases, axisymmetric waves form on the interface till achieving the apex known as capillary break up. After Dripping until the maximum break up length (u_{max}), the domain is determined axisymmetric flow. By increasing jet velocity, three-dimensional flow mode commences (see Fig. 2) wherein asymmetric waves are formed. Also, an atomization mode appears by approaching larger velocities [Kitamura *et al.* \(1982\)](#).

Imposing harmonic disturbance to the jet surface is mandatory, to investigate the instability of jet column. From this perspective, growing disturbance rate influences jet parameters directly e.g., breakup length, frequency of the interface waves and formation of droplets and satellites. A theory known as growth rate of developing disturbance is elaborated in [Kitamura *et al.* \(1982\)](#), [Ashgriz \(2011\)](#), which investigated the size of droplets and satellites produced from following disturbances:

- Utilizing acoustic waves on the interface of jet,
- Applying high voltage electric field via generating alternative contraction and expansion,
- Imposing oscillated flow,
- Enforcing periodic heaters,
- Changing the surface tension of the liquid jet.

Jet velocity and wavelength of disturbance are the main factors for droplets and satellites formation. As it is depicted in Fig.3 for high velocity jet, both droplets and satellites are formed. In contrast, for low velocity jet and high frequent disturbance, only droplets are formed. Electric field influences on disturbance, instability of jet and formation of droplets are studied in [Khoshnevis *et al.* \(2012\)](#), [Hokmabad *et al.* \(2014\)](#). In an experimental work, [Tabatabaee-Hosseini *et al.* \(2012\)](#) studied the colliding of two opposing jets under the same angle in the presence of electric field.

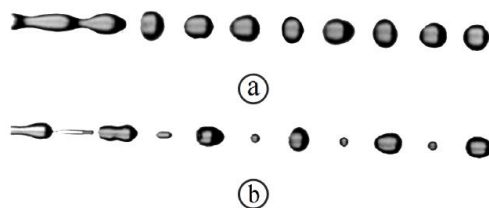


Fig. 3. a) Formation of only droplets due to uniform breakup of liquid jet column with low velocity and high frequent disturbance, b) formation of droplets and satellites simultaneously, due to unstable liquid column jet with high velocity and low frequent disturbance.

Charge induction is a suitable approach to change the liquid jet surface tension. The electrostatic repulsive force caused by free charges on the jet surface tends to decrease the liquid surface tension that yields a sooner jet break-up in comparison to

uncharged models. This related technique is widely applied to electrostatic spray [Cloupeau and Prunet-Foch \(1990\)](#) for industrial and agricultural purposes. The theoretical work was pioneered by [Rayleigh \(1882\)](#), who developed a theory of stability for electrified inviscid jets –subjected to disturbances of infinite wavelength –flowing in vacuum region. [Basset \(1894\)](#) studied the stability of axisymmetric disturbances on charged Newtonian jets under the effects of viscosity and the ambient gas. Later, [Taylor \(1969\)](#) corrected errors of Basset analysis. [Schneider *et al.* \(1967\)](#) experimentally verified the axisymmetric theoretical results by observing the breakup of a charged water jet through a grounded cylindrical electrode. [Huebner \(1969\)](#) also conducted a series of experiments on charged water jets. This study showed that increasing the amount of electricity enhances the growth of sinuous non-axisymmetric disturbances. Numerical simulations describe details of vorticity dynamics and clarified its mechanisms as well as effects of heat transfer on behaviour of non-circular jets. [Koshigoe and Tubis \(1986\)](#), [Koshigoe and Tubis \(1987\)](#), [Koshigoe *et al.* \(1988\)](#) analyzed the instability of jets with general shape and proposed a Greens function technique and a generalized shooting method. Recent studies of [Kasyap *et al.* \(2009\)](#) showed that a liquid jet emanating from an elliptic nozzle exhibits more unstable behavior or a faster breakup than a corresponding circular liquid jet. Furthermore, they found that decreasing aspect ratio (ratio of minor to major axis) of the elliptic nozzle in some ranges makes the elliptic liquid jet more unstable. Instability of an inviscid elliptic liquid jet in an inviscid gas has been investigated analytically by [Dityakin \(1954\)](#). By neglecting the gravity effects and considering the gas density, a 3-D temporal dispersion equation was derived. Later on, [Bechtel *et al.* \(1988\)](#) developed a one-dimensional model for slender viscoelastic elliptic liquid jets and used the predicted axis-switching behavior to measure dynamic surface tension and elongational viscosity of fluids. In a subsequent article, [Bechtel \(1989\)](#) studied viscosity and gravity effects on an elliptic jet in detail.

In this paper, nozzle geometry effects on excited liquid jets are investigated. Among possible asymmetric shapes, elliptic, equilateral triangular and quadrangular nozzles are selected. Geometrically, these jets are considered as the cases which clarify the effect of nozzle configuration on the flow behavior. By using these nozzle configurations, we analyze the surface energy and its influence on the exhausted liquid jet properties. Here, two different propulsion methods, i.e., charged and viscose jets, are utilized in order to excite exhausted jet. Both of these methods which are established on variation of fluid properties are new methods for the manipulation of axis-switching. The important properties of excited jets are compared for three different non-circular nozzles. which makes it possible to analyze the effects of corners (segments of greater curvature) on the instability of jet.

2. PHYSICS OF THE PROBLEM AND GOV ERNING EQUATIONS

In addition to the main equations, it is suggested to benefit auxiliary equations originated from the physics of experimental investigation. Hence, the Navier-Stocks equations for this case are as follows:

$$\nabla \bar{V} = 0 \quad (1)$$

$$\frac{\partial u_i}{\partial t} + u_j \frac{\partial u_i}{\partial x_j} = -\frac{1}{\rho} \frac{\partial P}{\partial x_i} + \nu \frac{\partial^2 u_i}{\partial x_j^2} + g + \frac{F_i}{\rho}$$

(2)

Eqs. (1)-(2) represent continuity and momentum equations, respectively. In these equations, u , P , $\nu = \mu/\rho$, ρ , g and F_i demonstrate velocity component in direction of jet flow, pressure inside the fluid, kinematic viscosity of the flow, density, acceleration of gravity and other body forces caused by external fields in the given order.

By utilizing necessary scales for variables and excluding the hydrodynamical forces where other body forces are ignored, non-dimensional numbers are proposed as:

$$Re = \frac{\rho D_h U_j}{\mu}, We = \frac{\rho D_h U_j^2}{\sigma}, Fr = \frac{U_j^2}{g D_h}$$

(3)

Re , We and Fr indicate Reynolds, Weber and Froude numbers in liquid jet which represent buoyancy, surface tension and gravity forces, respectively. Tension balance for liquid-gas interface has a great influence on jet instability which is defined:

$$(P_s - P_l + \sigma_{j-s} \cdot K) \bar{n} = (\tau_s - \tau_l) \bar{n} \quad (4)$$

where τ , $\bar{n} \rightarrow$, σ_{j-s} and K show stress tensor, unit normal vector on interface, surface tension in interface and mean curvature factor of jet's surface. In order to obtain σ_{j-s} and K , following equations are purposed:

$$\sigma_{j-s} = \sigma_j + \sigma_s - 2\sqrt{\sigma_j \sigma_s} \quad (5)$$

$$K = \frac{1}{R_1} + \frac{1}{R_2} \quad (6)$$

where σ_j and σ_s are the surface tension of the jet and base flows and R_1 and R_2 are radii of the jet's cross section curvature.

To illustrate all effects of instability based on mean values and their disturbances, we use:

$$\begin{aligned} u &= \bar{u} + u', v = \bar{v} + v' \\ p &= \bar{p} + p', R = a + \zeta \end{aligned} \quad (7)$$

where u and v are in the longitudinal and radial jet velocity. p is jet pressure, a is the mean radius and ζ is the disturbance of mean radius caused by instability. Eq. (7) rely on time because the disturbances of instabilities (prime variables) are time-dependent. Note that mean values do not depend on time. By utilizing the values of Eq. (7) and

revising continuity and Navier-Stocks equations, non-linear equations can be written as linear ones in cylindrical coordinate as:

$$\frac{1}{r} \frac{\partial r v'}{\partial r} + \frac{\partial u'}{\partial x} = 0, \frac{\partial u'}{\partial t} = -\frac{1}{\rho} \frac{\partial p'}{\partial x}, \frac{\partial v'}{\partial t} = -\frac{1}{\rho} \frac{\partial p'}{\partial r} \quad (8)$$

Eqs. (8) can be solved by means of analytical methods which leads to jet surface curvature equations in terms of its disturbance [Das \(1997\)](#):

$$\frac{1}{R_1} = \frac{1}{a + \zeta}, \frac{1}{R_2} = \frac{-\zeta_{xr}}{(1 + \zeta_x^2)^{3/2}} \quad (9)$$

here, ζ_{xr} shows jet interface function and ζ_x depicts the interface curvature function of main direction of jet. According to the Eqs. (9), non-linear time-dependent liquid flow pattern can be analytically solved in particular circumstances for the circular nozzle. This pattern fails to be used for non-circular jets, therefore, they do not have any specific analytical solution. On the other hand, for non-circular jets, the theoretical jet cross section is given in polar coordinate by [Rayleigh \(1879\)](#). In order to find the radial distance of the jet, we have:

$$R = a_0 + a_n \cos n\theta \quad (10)$$

where θ , a_0 and a_n are the angular coordinate, the mean radius of jet and amplitude of the instability. The wavelength of jet oscillation is written as follow:

$$\lambda = \frac{2\pi U_j}{p} \quad (11)$$

where p is the thermal frequency of jet instability.

By assuming that an is diminutive comparing to a_0 , the non-dimensionalized wavelength of jet instability for non-circular jets is calculated as below [Kasyap *et al.* \(2009\)](#), [Amini and Dolatabadi \(2012\)](#), [Wang and Fang \(2015\)](#):

$$\frac{\lambda}{D} = \frac{\pi}{\sqrt{2(n^3 - n)}} We^{0.5} \quad (12)$$

In this equation n is the number of undulations in the cross section of the jet which is 2, 3, and 4 for elliptical, triangular and square jets, respectively.

3. EXPERIMENTAL SETUPS

Non-circular jets are highly significant due to producing instabilities originated from contracting and expanding jet interface as well as satellites and droplets creation. [Ho and Gutmark \(1987\)](#), [Baty and Morris \(1995\)](#) have depicted the notable application of these jets.

In order to study the nozzle geometry, four sets of stainless steel nozzles with different geometries and approximately same cross sectional areas were manufactured (by a wire-cut electro discharge machining process) and tested (see Fig. 4). The geometric details of the nozzles are given in Table 1. The Hydraulic diameter of the nozzles, D_h is estimated as $D_h = 4A/P$, that A is nozzle exit area and P is wetted perimeter.

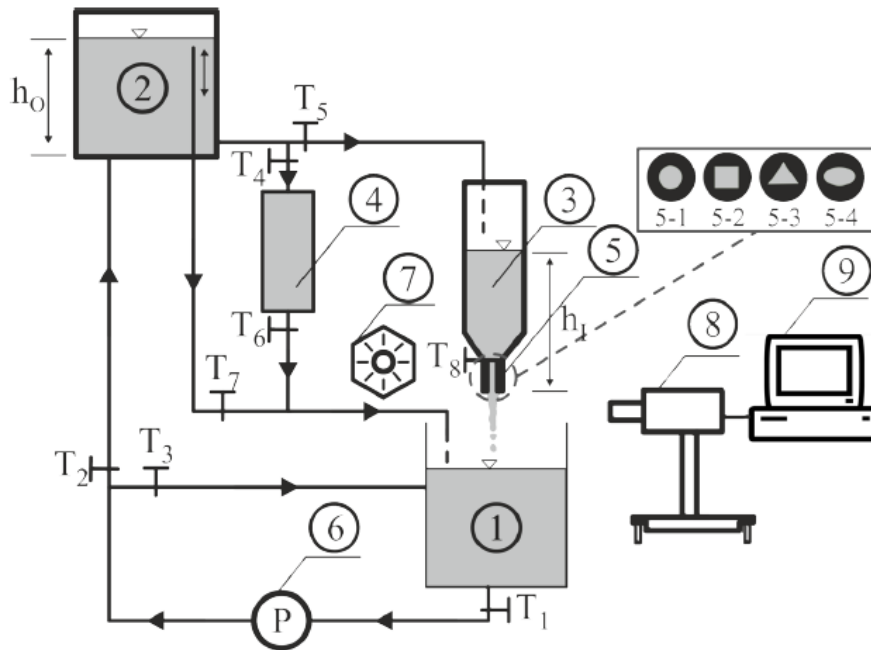


Fig. 4. Schematic setup of free-jet investigation in silent medium, 1. Main tank, 2. Head tank, 3. Feed tank, 4. Sampling tank, 5. Nozzle, 5-1. Circular nozzle, 5-2. Square nozzle, 5-3. Triangular nozzle, 5-4. Elliptic nozzle, 6. Head supply tank, 7. Extended light source, 8. Camera, 9. Data processor system, Flow control taps (T_i).

Table 1 Geometrical details of utilized nozzles

| Nozzles | Geometry | Dim. (mm) | D_h (mm) |
|------------------------|----------|-----------------|------------|
| Elliptical | | a=4.43 , b=1.49 | 2.57 |
| Equilateral triangular | | a=4.45 | 2.57 |
| Quadrangular | | a=2.57 | 2.57 |
| Circular | | D=2.57 | 2.57 |

Experiments were carried out with distilled water for the first method of excitation (charged jet). While in the second method of excitation, different fluid solutions of water-glycerol mixture were utilized to generate viscosity variations. In Table 2, physical properties of operating fluids are shown. For calculating σ_{mix} (surface tension of mixture) in water-glycerol with different solutions, we use following equation:

$$\sigma_{mix} = \phi\sigma_w + (1-\phi)\sigma_{GI} \quad (13)$$

where Φ is volume fraction of solution and other subscriptions of σ represent water (w) and glycerol (GI).

A setup (see Fig. 4) is designed in a way that jet flow will be in a steady state. During experiments, nozzles are fixed in a feed tank with 50 mm diameter and 300 mm length to supply the essential hydrostatic back pressure. First, liquid flows appropriate to the output

jet velocity and reaches the constant height in head tank (h_0). Then, for controlling feed tank's head (h_1), it overflows from the head tank to the main tank. A control valve is used to supply experimental fluids from the head tank to the feed tank to create jet flow with adequate quantity of velocity.

In the present work, jet velocity is computed via two measurement methods; The first one is direct discharge using sampler tank (sampling by time) and the second one is the flow rate considering the flow motion continuity with nozzles cross sections area. By stabilizing head of feed tank (h_1) and applying Torricelli's equation, output velocity is calculated by:

$$U_j = \sqrt{2gh_1} \quad (14)$$

The experiments are performed in two different sections. In the first part, the behavior of non-circular charged water jets are studied; and in the second part,

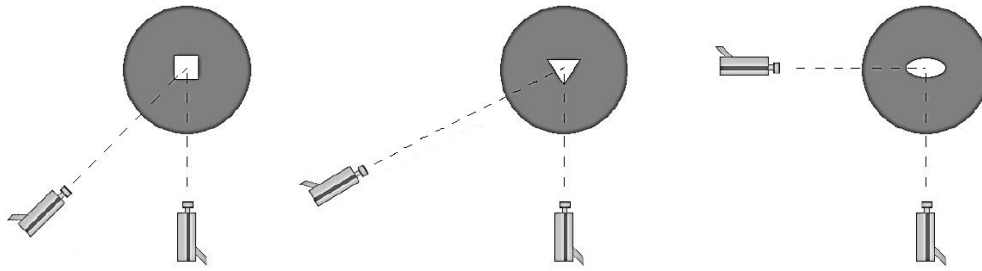


Fig. 5. Camera views for non-circular nozzles.

Table 2 Physical properties of working fluids

| Utilized fluids | $\rho(kg/m^3)$ | $\mu(kg/(m \cdot s))$ | $\sigma(N/m)$ |
|-----------------------------|----------------|-----------------------|---------------|
| Distilled water | 998 | 8×10^{-4} | 0.073 |
| GL1(70% water+30% glycerol) | 1068 | 1.87×10^{-3} | 0.070 |
| GL2(50% water+50% glycerol) | 1121 | 4.21×10^{-3} | 0.069 |
| GL3(30% water+70% glycerol) | 1176 | 14.1×10^{-3} | 0.068 |

effects of viscosity on the behavior of emanated jets are analyzed. In the former, the electrical charge is conducted on the jet surface through a high voltage power supply.

A 500 W halogen floodlight is used to illuminate the jet flows and a high-speed CCD color video camera (Casio EXF1) at a frame rate up to 1200 fps and with a resolution of about 900 dpi was utilized during imaging process. For each of nozzle geometries, two sets of images were taken by 0 and $\pi/2$ angles for elliptical, 0 and $\pi/3$ for tri-angular, and 0 and $\pi/4$ for square to observe the axis-switching phenomenon clearly. These camera views are schematically showed in Fig. 5. Furthermore, images were extracted from the recorded videos for subsequent analysis. In the end, we substitute the data to Image Pro Plus (IPP) software for detailed evaluation.

4. MEASUREMENTS AND UNCERTAINTY

Flow discharge for two mentioned experiment sets is gained with high accuracy via the direct method which is done by sampling Coleman and Steele (2009). Hence, the volume flow rate (q_v) and jet velocity (U_j) are defined as following,

$$q_v = \frac{V}{t} \tag{15}$$

$$U_j = \frac{4q_v}{\pi D_h^2} = \frac{4V}{\pi D_h^2 t} = KV t^{-1} D_h^{-2}$$

The measurement sensitivity of volume (V), time (t) and nozzles hydraulic diameter (D_h) are 0.4%, 0.5% and 1% in the given order. By considering Eq. (16), uncertainty for the jet velocity is in the acceptable value as 2.4%.

$$U_{U_j} = \frac{\delta U_j}{U_j} = 2.4\% \tag{16}$$

In analyzing the results, Re and We are two fundamental parameters that their uncertainties are writ-ten as below:

$$We_j = \frac{\rho_j U_j^2 D_h}{\sigma} = \rho_j U_j^2 \cdot D_h \cdot \sigma^{-1} \tag{17}$$

$$Re_j = \frac{\rho_j U_j D_h}{\mu} = \rho_j U_j \cdot D_h \cdot \mu^{-1}$$

Here, errors of constitutive variables for these parameters are noted in Table 3. As it is seen, uncertainty for Re and We are 4% and 3.3%, respectively.

5. RESULTS AND DISCUSSIONS

The breakup length, penetration depth and wavelength of axis-switching beside frequency and sizes of the produced droplets and satellites are the main parameters investigated in this paper. As aforementioned, for studying nozzles geometry effects, video records and image processing are used. Fig. 6 illustrates breakup length for elliptical and triangular nozzles with distilled water.

For all studied non-circular liquid jets, a lower limit of We number prevents axis-switching. Fig. 7 presents images of liquid jets discharging in these conditions. This figure reveals that the axis-switching phenomenon does not show itself and jets degenerate to circular shape immediately after exiting from nozzles.

Dominance of surface tension forces compels the jet to take a circular cross section to minimize its surface energy and leads to the suppression of axis-switching process. With the glycerol addition, viscosity acts as a dampening agent and besides the surface tension forces overcome the inertial one. Therefore, the axis-switching starts to become visible at a threshold value of We which is denoted by We_{min} in this paper. As We passes the thresh-old value, the lateral inertia

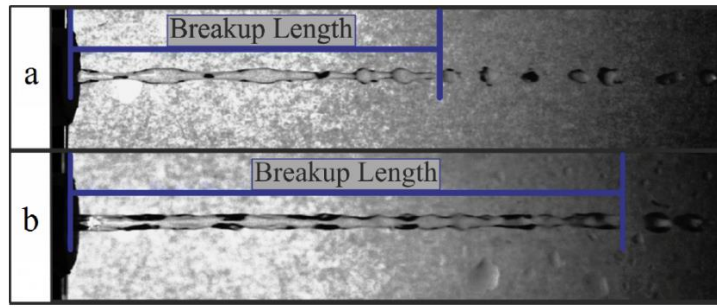


Fig. 6. Breakup length of distilled water jet for a) elliptical and b) triangular nozzles.

Table 3 Physical properties of working fluids

| Errors | Value | Uncertainty | Value |
|------------------------|-------|-------------------------------|-------|
| $\delta D_h/D_h$ | 0.04% | $U_{We_j} = \delta We_j/We_j$ | 4.84% |
| $\delta \sigma/\sigma$ | 0.04% | $U_{Re_j} = \delta Re_j/Re_j$ | 2.69% |
| $\delta \rho_j/\rho_j$ | 0.6% | | |
| $\delta U_j/U_j$ | 2.4% | | |
| $\delta \mu/\mu$ | 1.06% | | |

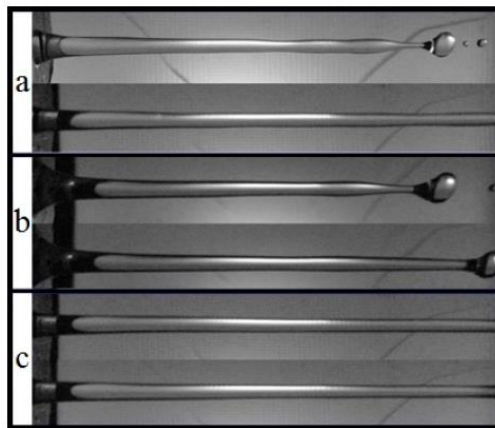


Fig. 7. Non-circular liquid jets discharging from a) elliptical, b) triangular and c) quadrangular nozzles.

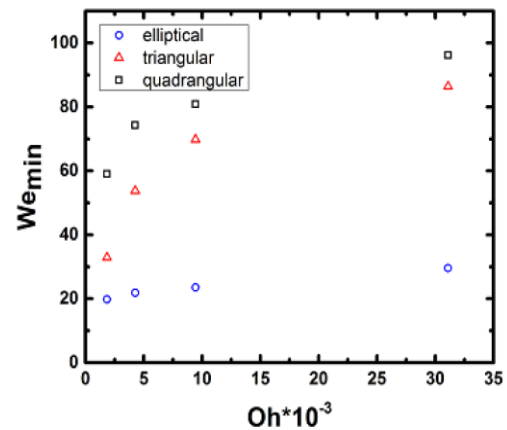


Fig. 8. Variation of We_{min} as a function of Oh for elliptical, triangular and quadrangular nozzles.

of the liquid jet also increases and becomes comparable to surface tension forces and jet's viscosity. At this point, according to [Tabatabaee-Hosseini et al. \(2012\)](#), the free surface of the jet behaves like a stretched membrane which executes oscillations in the lateral direction and develops axis-switching.

The effect of liquid jet viscosity for this analysis is noticeable with emerging Ohnesorge number:

$$oh = \frac{\mu}{(\rho\sigma D)^{1/2}} = \frac{We_{min}^{1/2}}{Re} \quad (18)$$

In quadrangular cross-section, We_{min} has greater value than in triangular and elliptical ones. With Ohnesorge augmentation, the value of We_{min} is also increased, which is a good indicator for the predominance of viscosity forces (see Fig. 8).

To better understand the obtained experimental results, they are divided into two distinct parts; the former part discusses the jet behaviour before breakup and the latter part includes the characteristics of jet properties after breakup.

5.1 Liquid jets properties before breakup

Non-circular jets have higher mixing rate due to larger entrainment where it comes from axis-switching effect. In the present study, the decay length of axis-switching L_{as} demonstrates entrainment rate of non-circular jets. This length was defined as the distance measured from the nozzle exit to the point of axis-switching destabilization. The decay length depends on the intensity of surface tension and viscous forces, in charged jets and the second excited case respectively. It means, these opponent forces shorten the decay length in contrast to inertial force enhancing the axis-switching. The

mentioned length is illustrated in the Fig. 9 for the case of distilled water. Fig. 9 shows the penetration depth for three nozzle types i.e., elliptical, triangular and quadrangular in different We values.

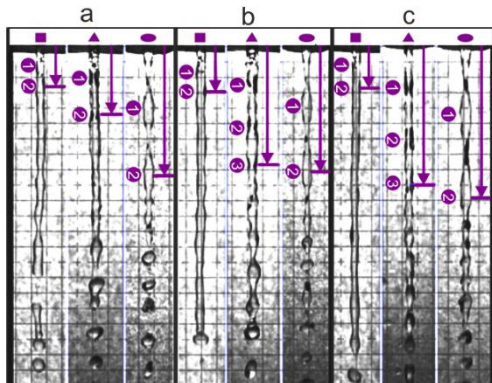


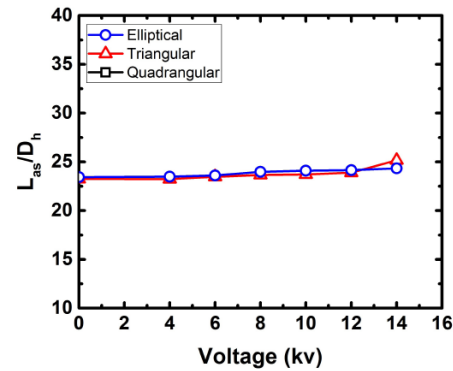
Fig. 9. Axis-switching penetration depth for a) $We= 59.15$, b) $We= 65.56$ and c) $We= 70.42$.

It can be concluded from Fig. 10 that increasing the applied voltage extends the decay length due to propagation of electrical charge on the jet surface and its repulsion forces. This fact is the major reason behind the variation of axis-switching wave-length. Moreover, it is clear that by adding the twin-vortex number, decay length decreases. We interpret that the elliptical nozzle with two twin-vortexes has a longer decay length comparing to the quadrangular one which has four. Also, for quadrangular jet, L_{as} in Fig. 10 a and b are not observed due to its higher We_{min} .

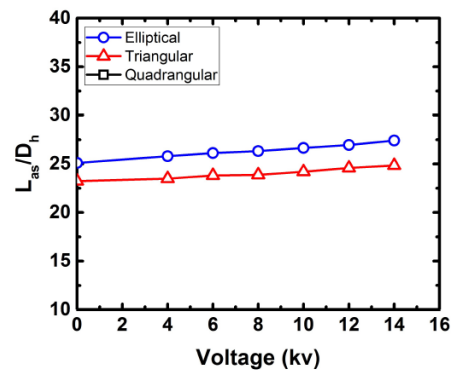
Figures 10 and 11 illustrate that the decay length increases with the Weber number augmentation in all studied nozzles for both excitation methods. It is noteworthy that in the second method of excitation, the decay length reduces with corners increment similar to charged jets. In the case of quadrangular jet, the axis-switching commences for higher Weber numbers, and this threshold value rises up with the viscosity augmentation. Accordingly, the decay length for quadrangular jet can be measured solely for distilled water (Fig. 11a).

The mechanism of liquid jet breakup is influenced by a wide range of parameters, including the in-let condition before the jet's emanation, the nozzle geometry, and the environmental situation into which the jet flows. Among all these affecting parameters, influence of the nozzle geometry has been overlooked in literatures despite the fact that nozzles with different shapes have already been considered for practical applications [Reitz and Bracco \(1982\)](#). The effect of nozzle geometry on the breakup length as well as its dependency on the number of corners are clarified throughout the current experiments. Here, the jet breakup length is defined as the distance measured from the nozzle exit to the point that jet breaks for the first time along its axis. Mean breakup length (L_b) was estimated from the individual measurements of jet breakup length obtained from photographs available for each flow condition. In the case of charged jets, attained values

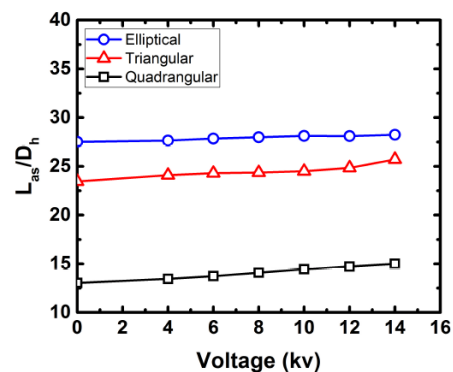
for this length do not have a distinctive trend.



a)



b)



c)

Fig. 10. Decay length variations as a function of applied electrical potential difference; a) $We=48.419$, b) $We=51.573$, c) $We=55.275$.

The casual behavior of breakup length is due to the combination of axisymmetric and asymmetric waves on the jet surface. Because the electrostatic repulsive forces produced by free charges on the jet surface tend to trigger the asymmetric disturbances, earlier breakup happens [Huebner and Chu \(1971\)](#).

Variations of L_b/D_h for liquid jets exhausting from three types of nozzles are depicted in the Fig. 12 for the second method of excitation. It can be seen that the viscosity stabilizes the jet and tends to increase the breakup length. In fact, viscosity is a factor that prevails over the pinching effect caused by surface tension, and delays the breakup point [Weber \(1931\)](#).

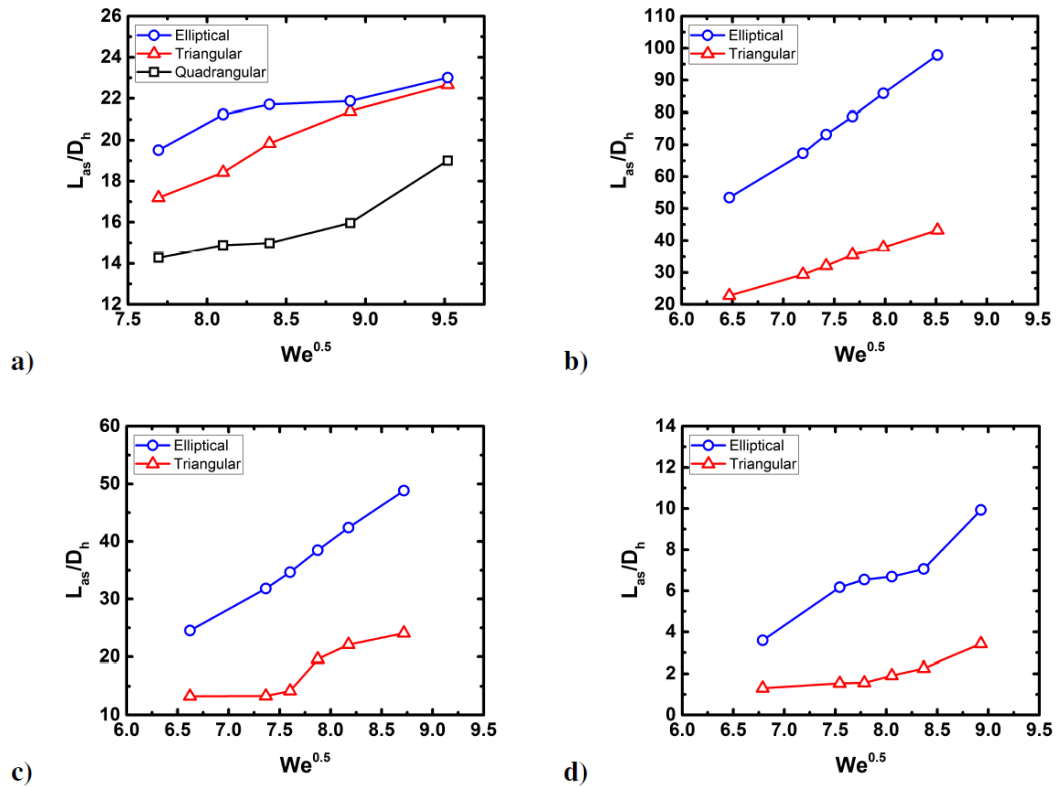


Fig. 11. Axis-switching declination length function of Weber number for a) distilled water, b) GL1, c) GL2 and d) GL3.

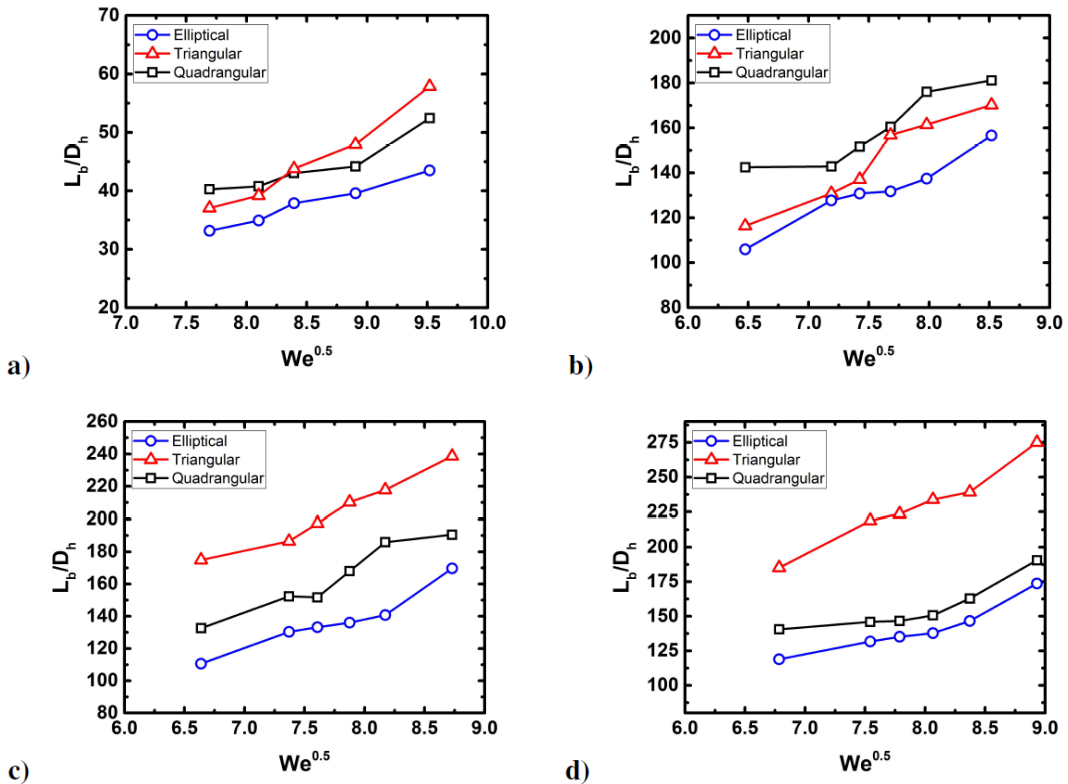


Fig. 12. Variation of non-dimensional breakup length as a function of $We^{0.5}$ in non-circular nozzles for utilized a) Distilled water, b) GL1, c) GL2 and d) GL3.

Fig. 12 reveals that in all used nozzles, unbroken length of the liquid jet increases with the flow rate augmentation. Also, it is clear from this figure that the breakup length of triangular nozzle is longer than elliptical nozzle for the whole range of $We^{0.5}$. This is due to twin-vortex number which is higher for triangular jet. Thus, increment of corner number is a factor in retarding the jet breakup. The recent result about the relationship between the breakup length and corners number stems from different surface energy level in each of nozzles. It is known that the surface energy of a circular liquid jet is lower than the surface energy of equivalent non-circular jets with axis-switching segments. Furthermore, ascending trend of surface energy carries out with the axis-switching segments propagation. On the other hand, a liquid jet or liquid ligament would disintegrate into spherical drops in order to reach a configuration with minimum surface energy. So, with increasing the number of axis-switching segments within the nozzle geometry, the surface energy of discharged liquid jet ascends and reaching the minimum surface energy takes much more time. The increasing trend of breakup length with the segments increment will face a problem in the case of quadrangular nozzle which will be more prominent by increasing the viscosity of jet, as can be seen in Fig. 12. The reason behind this abnormal behavior is the presence of transverse waves that appear on the jet surface after a critical value of We . Emerged waves destabilize the liquid jet. This phenomenon creates bigger segments which makes breakup length shorter. As a result, after a threshold value of We (We_{crit}) in quadrangular jet, transverse waves oppose liquid surface energy, and reduce its effect on increasing the breakup length. The growth of transverse waves on the quadrangular jets surface is shown in the Fig. 13 for two We numbers.

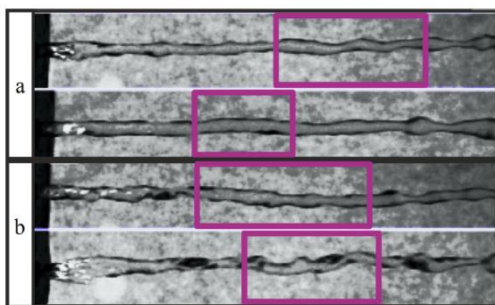


Fig. 13. Transverse waves detected on quadrangular jet for two We numbers in the same time interval, A) $We=79.304$, B) $We=90.684$.

As the viscosity augments, emerged transverse waves diminish. In this condition, dominant reason for disharmonic behavior of unbroken length of quadrangular jet comparing to the prior shapes is that the quadrangular jet behaves similar to the circular one. By increasing segments with greater curvature on the nozzle perimeter, its geometry approximate to circular form. Consequently, the quadrangular jet behaves like circular jet in upper viscosities. Also, a direct relation between the viscosity and this

phenomenon is verified.

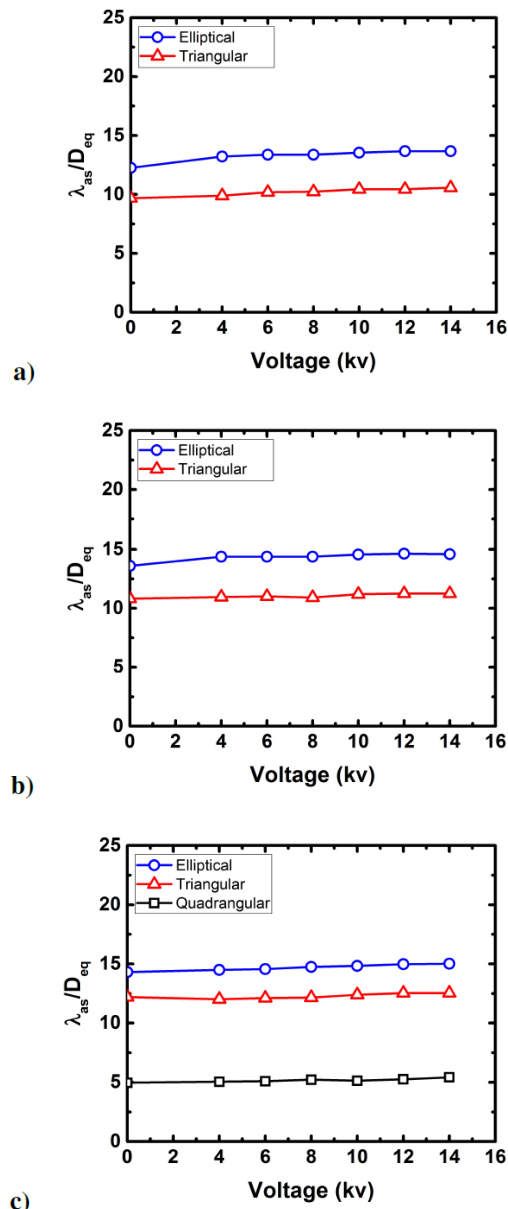


Fig. 14. Axis-switching wavelength variations (λ_{as}/D_{eq}) as a function of applied electric potential difference; a) $We=48.419$, b) $We=51.573$, c) $We=55.275$.

The wavelength of axis-switching (λ_{as}) is measured for all studied cases in both excitation means. By applying nozzles equivalent diameter (D_{eq}), which is obtained by $D_{eq} = \sqrt{(4A0)/\pi}$, non-dimensional axis-switching wavelength is calculated [Rajesh *et al.* \(2016\)](#). Variations of λ_{as}/D_{eq} as a function of Weber number for all nozzle geometries are depicted in two distinct parts i.e., electrical and viscosity excitation methods.

Increase in variation of λ_{as}/D_{eq} with applied voltage in the Fig. 14 was predictable, because the electrostatic repulsive forces caused by free charges on the jet surface tend to reduce the surface tension.

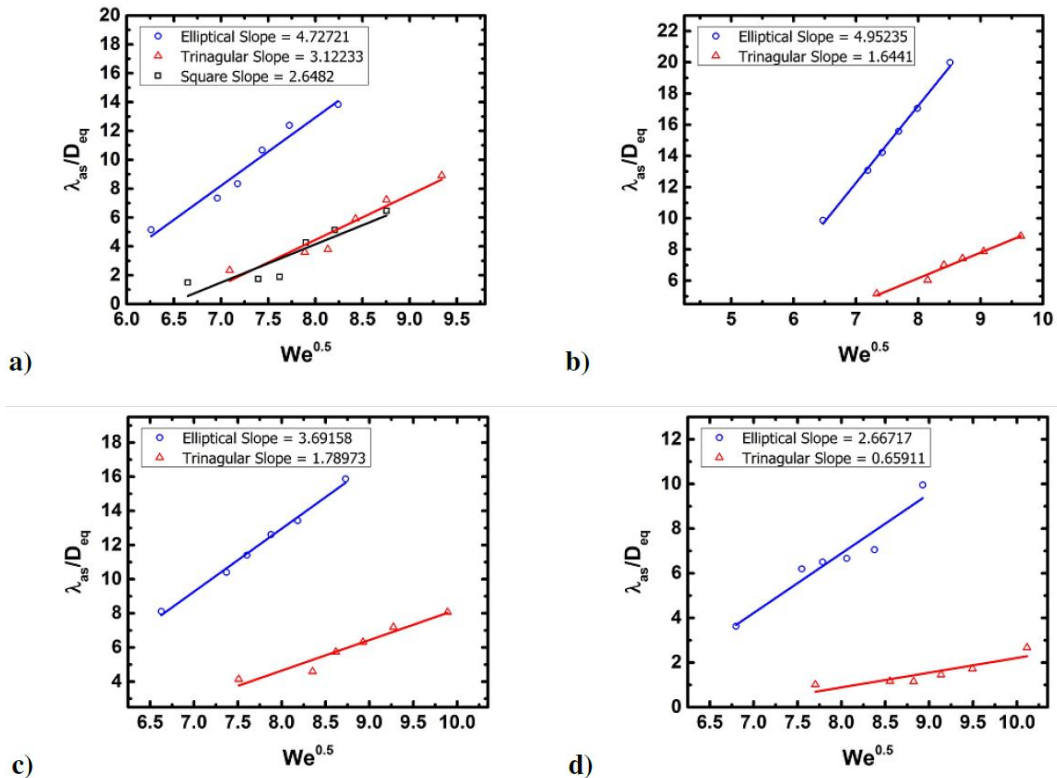


Fig. 15. Axis-switching wavelength variations (λ_{as}/D_{eq}) as a function of $We^{0.5}$ number for all utilized fluids; a) distilled water, b) GL1, c) GL2, d) GL3.

Since, the surface tension is a deterrent force against the axis-switching, increasing the amount of electrical charges on the jet surface prolongs the axis-switching and its wavelength. Also, we observe that the linear trend of λ_{as}/D_{eq} with applied voltage holds true for all nozzle geometries. In all studied flow rates, the wavelength of axis-switching will decrease with the increment of twin-vortexes number. It means, elliptical nozzle with two twin-vortexes has a bigger wavelength in comparison to quadrangular one which has four.

The plots of λ_{as}/D_{eq} for water and waterglycerol mixture jets show a linear variation which is consistent with the previous observations (Rayleigh 1879, Rajesh *et al.* 2016). Fig. 15 illustrates the linear trend of λ_{as}/D_{eq} with $We^{0.5}$ is accurate for all nozzles and the nozzle geometry does not seem to influence it. As aforementioned, the value of We_{min} for the case of quadrangular nozzle is upper than others, so measurements of λ_{as} for quadrangular jet was limited to a narrow range of We numbers, and will be more narrow with the viscosity augmentation. Therefore, λ_{as}/D_{eq} for this geometry covers a short range of We and is not suitable to illustrate properties after breakup.

5.2 Characterization of Excited Liquid Jets

Due to the effect of applied excitations and nozzle geometry on the produced droplets, the second part of experiments is assigned to the pinched droplets. These properties include droplet formation

frequency beside droplet and satellite diameter variations for different nozzle geometries and working liquids. Owing to the ordinary breakup behavior of charged jets, it was not possible to get a definite behaviour for the liquid jet properties after pinch-off. Therefore, this part represents the obtained results interpreted from the second excitation method.

Fig. 16 shows that droplet formation frequency raises with the velocity increment which can be explained by considering inertial forces. Further-more, propagation of glycerol amount in the solution (increasing the jet viscosity) enhances the viscous forces against the inertial ones and as a result, the formation frequency of droplet decreases.

Because of droplet size fluctuation, a minimum of 150 droplets for each solution of water-glycerol mixtures and flow rates were measured and the average size is reported in each situation. The diameter is recorded only when it had been separated from the jet completely and formed approximately a spherical shape. Fig. 17 depicts variation of non-dimensional droplet mean diameter for all utilized non-circular nozzles as a function of Weber number for different jet viscosity. This figure reveals, produced droplets from triangular jet are bigger compared to square and elliptical ones for the whole range of Weber numbers and different viscosities. Increment in corners or segments (twin-vortexes number) postpones the jet breakup while increases the mean diameter of detached droplets. The size of

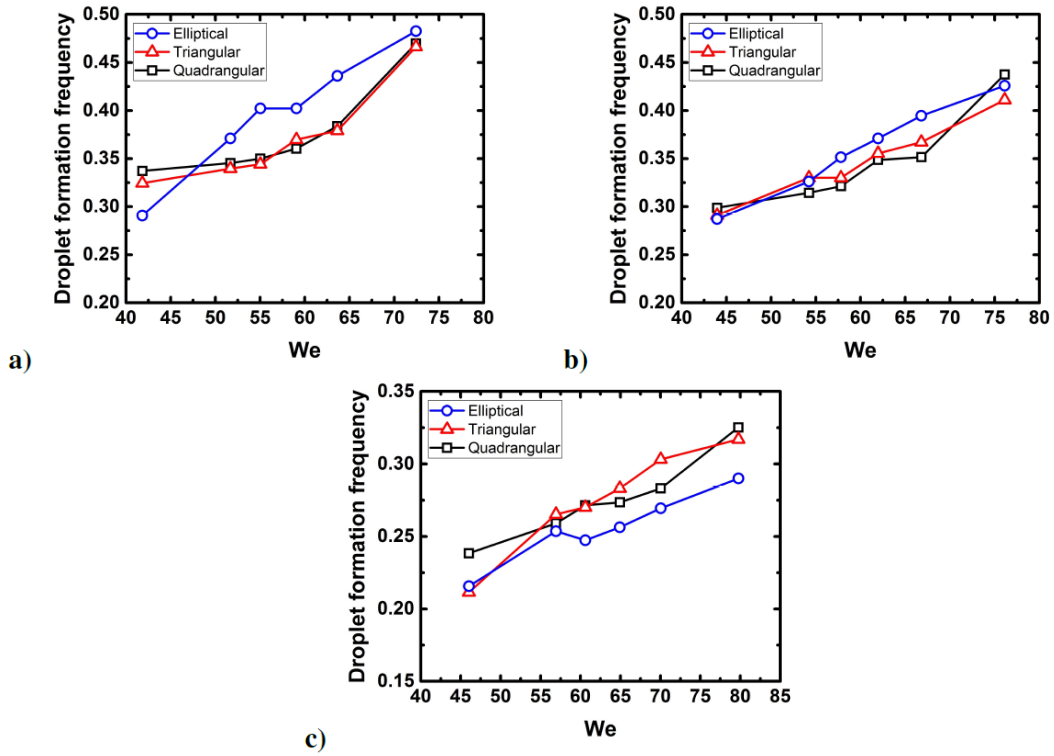


Fig. 16. Variation of droplet formation frequency over We number for elliptical, triangular and quadrangular nozzles with a) GL1, b) GL2 and c) GL3.

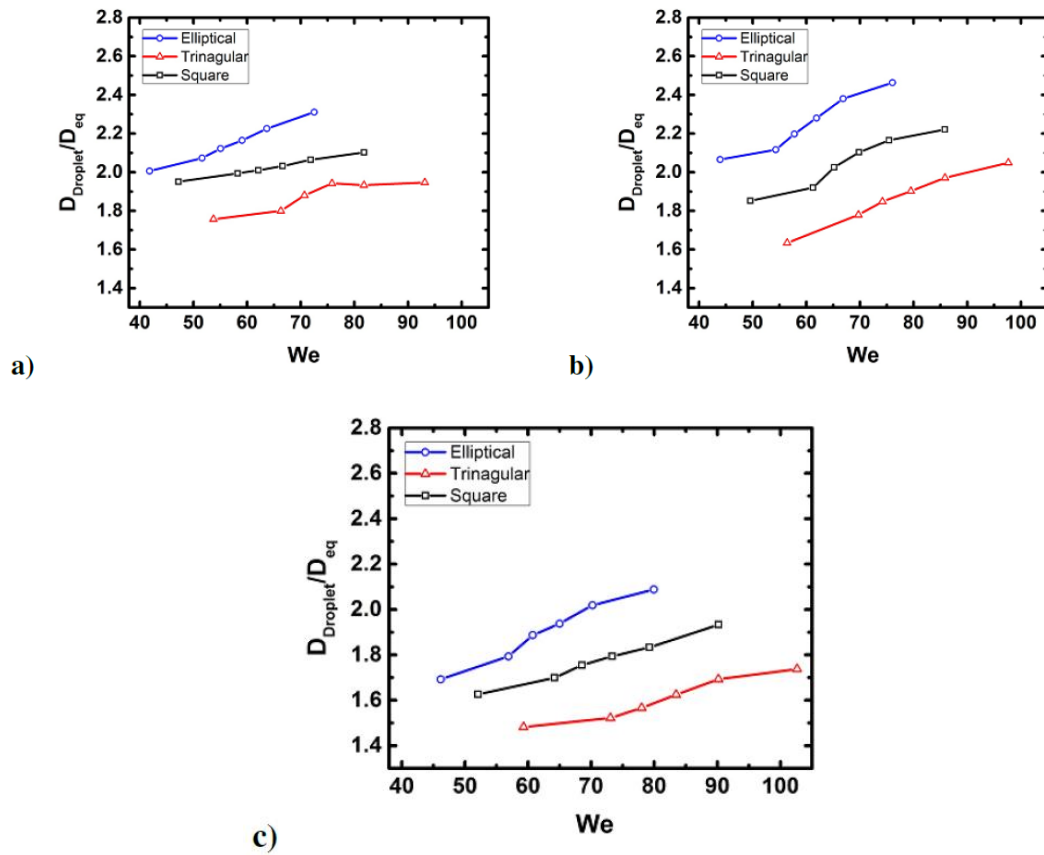


Fig. 17. Non-dimensional droplet diameter as a function of We number; a) GL1, b) GL2, c) GL3.

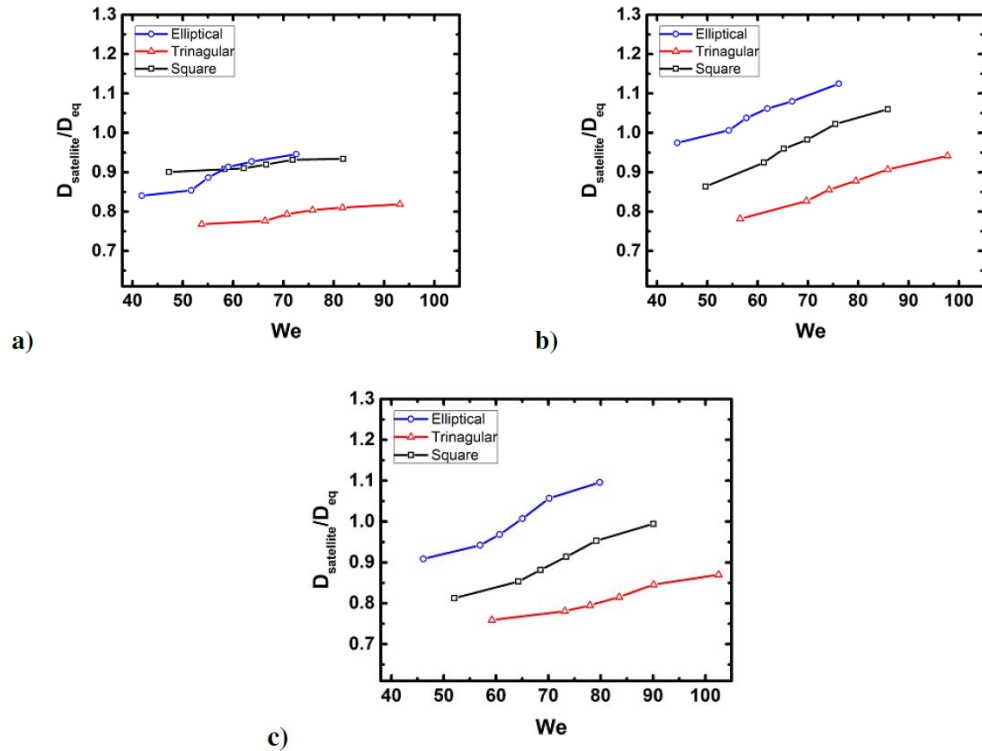


Fig. 18. Non-dimensional satellite diameter for different We numbers; a) GL1, b) GL2, c) GL3.

disintegrated droplets is in a direct proportion with breakup length. Hence, the increasing trend of droplet diameter will face a problem in the case of quadrangular nozzle. The nozzle geometry which approaches the circular shape is the main reason for the mentioned inconsistency. It makes exhausted liquid jets to reach the minimum inter-face energy configuration sooner. Consequently, the breakup takes place sooner and droplets fail to grow completely.

From Fig. 18, effects of jet velocity and nozzle geometry on satellite formation are vivid. Two important points can be obtained from this figure; the former is the growth of satellites with increment of the flow rate, and the latter is the relation between satellite diameter and the number of corners (segments with greater curvature) on the nozzle perimeter. Both satellite and mean droplet have similar trends over We number for various nozzle geometries. Therefore, by corners augmentation, satellite size becomes bigger except for quadrangular nozzle.

6. CONCLUSION

Discharged liquid jet from three different non-circular nozzles –with approximately same cross section areas–has been studied experimentally. Two different methods which were based on the variation of liquid properties have been applied to excite exhausted jets. Identical experiments are conducted for all nozzle geometries in both excitation methods. The axis-switching process of non-circular liquid jets is investigated in the present study by measuring the

jet axis-switching wave-length. Based on the present work, main conclusions could be drawn as below:

- For both propulsion methods, as We increases, the decay length of axis-switching L_{as} raises, however, increasing the number of twin-vortexes decreases this length. Also, charged jets with higher applied voltages have longer decay lengths.
- Breakup length, as an important parameter for jets, lacks a uniform trend for the first exciting mean. On the other hand, for viscous liquid jets, it is raised by augmentation of the We number.
- The unbroken length of viscous jets for nozzle with more twin-vortex number is higher except for quadrangular one, where transverse waves appear on its surface.
- The wavelength of axis-switching increases proportionally with the applied voltage and flow rate. Inversely, viscosity acts as a deterrent unit and reduces its wavelength. Moreover, for both excitations, elliptical jets have greater axis-switching wavelength in comparison to triangular and quadrangular jets.
- The increment of We number leads to produce more droplets and consequently higher formation frequency of droplets. In contrast, viscosity has a negative impact on droplet production frequency.
- The droplet and satellite diameters are in direct relation with We number. As We number goes up, the mean diameter of droplets and satellites

rise. Elliptical jets have bigger droplets and satellites comparing to quadrangular jets, while triangular jets possess the smallest ones.

REFERENCES

- Amini, G. and A. Dolatabadi (2011). Capillary instability of elliptic liquid jets. *Physics of Fluids* 23(8), 084109.
- Amini, G. and A. Dolatabadi (2012). Axis-switching and breakup of low-speed elliptic liquid jets. *International Journal of Multi-phase Flow* 42, 96–103.
- Amini, G., Y. Lv, A. Dolatabadi and M. Ihme (2014). Instability of elliptic liquid jets: Temporal linear stability theory and experimental analysis. *Physics of Fluids* 26(11), 114105.
- Ashgriz, N. (2011). *Handbook of atomization and spray*. Springer.
- Basset, A. B. (1894). Waves and jets in a viscous liquid. *American Journal of Mathematics* 16(1), 93–110.
- Baty, R. S. and P. J. Morris (1995). The instability of jets of arbitrary exit geometry. *International Journal for Numerical Methods in Fluids* 21(9), 763–780.
- Bechtel, S. (1989). The oscillation of slender elliptical inviscid and newtonian jets: Effects of surface tension, inertia, viscosity and gravity. *Journal of Applied Mechanics* 56, 968–974.
- Bechtel, S., M. Forest, D. Holm and K. Lin (1988). One-dimensional closure models for three-dimensional incompressible viscoelastic free jets: von kármán flow geometry and elliptical cross-section. *Journal of Fluid Mechanics* 196, 241–262.
- Cloupeau, M. and B. PrunetFoch (1990). Electrostatic spraying of liquids: main functioning modes. *Journal of electrostatics* 25(2), 165–184.
- Coleman, H. W. and W. G. Steele (2009). *Experimentation, Validation, and Uncertainty Analysis for Engineers*. John Wiley and Sons, Inc.
- Crighton, D. (1973). Instability of an elliptic jet. *Journal of Fluid Mechanics* 59(4), 665–672.
- Das, T. K. (1997). Prediction of jet breakup length in liquid-liquid systems using the Rayleigh-Tomotika analysis. *Atomization and Sprays* 7(5), 549–559.
- Dityakin, Y. F. (1954). On the stability and breakup into drops of a liquid jet of elliptical cross section. *Izv. Akad. Nauk SSSR, Otdel. Tekhn. Nauk* 10, 124–130.
- Gutmark, E., K. C. Schadow and C. J. Bicker (1990). Near acoustic field and shock structure of rectangular supersonic jets. *AIAA Journal* 28(7), 1163–1170.
- Gutmark, E., K. C. Schadow, T. P. Parr, D. M. Hanson-Parr and K. J. Wilson (1989). Non-circular jets in combustion systems. *Experiments in Fluids* 7(4), 248–258.
- Ho, C. and E. Gutmark (1987). Vortex induction and mass entrainment in a small-aspect-ratio elliptic jet. *Journal of Fluid Mechanics* 179, 383–405.
- Hokmabad, B. V., S. Faraji, T. G. Dizajyekan, B. Sadri and E. Esmaeilzadeh (2014). Electric field-assisted manipulation of liquid jet and emanated droplets. *International Journal of Multiphase Flow* 65, 127 – 137.
- Huebner, A. (1969). Disintegration of charged liquid jets. *Journal of Fluid Mechanics* 38(4), 679–688.
- Huebner, A. and H. Chu (1971). Instability and breakup of charged liquid jets. *Journal of Fluid Mechanics* 49(2), 361–372.
- Kandjani, A. E., A. Khoshnevis, M. Hemayatkhah, E. Esmaeilzadeh, M. Vaezi and M. Eslamian (2010). Powder production via electrohydrodynamic-assisted molten metal jet impingement into a viscous medium. *Powder Technology* 203(3), 518 – 528.
- Kasyap, T., D. Sivakumar and B. Raghunandan (2008). Breakup of liquid jets emanating from elliptical orifices at low flow conditions. *Atomization and Sprays* 18(7).
- Kasyap, T., D. Sivakumar and B. Raghunandan (2009). Flow and breakup characteristics of elliptical liquid jets. *International journal of multiphase flow* 35(1), 8–19.
- Khoshnevis, A., M. F. Tabriz, M. Hemayatkhah, A. E. Kandjani, J. M. Milani, E. Esmaeilzadeh, M. Eslamian and M. R. Vaezi (2012). Characteristics of the breakup and fragmentation of an electrohydrodynamic melt jet. *Particuology* 10(3), 255 – 265.
- Khoshnevis, A., S. S. H. Tsai and E. Esmaeilzadeh (2014). Electric field induced sheeting and breakup of dielectric liquid jets. *Physics of Fluids* 26(1), 012103.
- Kitamura, Y., H. Mishima and T. Takahashi (1982). Stability of jets in liquid-liquid systems. *The Canadian Journal of Chemical Engineering* 60(6), 723–731.
- Koshigoe, S. and A. Tubis (1986). Wave structures in jets of arbitrary shape. i. linear inviscid spatial instability analysis. *The Physics of fluids* 29(12), 3982–3992.
- Koshigoe, S. and A. Tubis (1987). Wave structures in jets of arbitrary shape. ii. application of a generalized shooting method to linear instability analysis. *The Physics of fluids* 30(6), 1715–1723.
- Koshigoe, S., E. Gutmark, K. C. Schadow and A. Tubis (1988). Wave structures in jets of arbitrary shape. iii. triangular jets. *The Physics of Fluids* 31(6), 1410–1419.

- Lee, S.J. and S. J. Baek (1994). The effect of aspect ratio on the near-field turbulent structure of elliptic jets. *Flow Measurement and Instrumentation* 5(3), 170–180.
- Muthukumar, C. and A. Vaidyanathan (2014). Experimental study of elliptical jet from sub to supercritical conditions. *Physics of Fluids* 26(4), 044104.
- Nuytens, D., M. D. Schampheleire, P. Verboven and B. Sonck (2010). Comparison between indirect and direct spray drift assessment methods. *Biosystems Engineering* 105(1), 2 – 12.
- Nuytens, D., M. De Schampheleire, W. Steurbaut, K. Baetens, P. Verboven, B. Nicolai, H. Ramon and B. Sonck (2006). Experimental study of factors influencing the risk of drift from field sprayers part 2: Spray application technique. *Aspects of Applied Biology* 77(2), 331–339.
- Quinn, W. (1989). On mixing in an elliptic turbulent free jet. *Physics of Fluids A: Fluid Dynamics* 1(10), 1716–1722.
- Rajesh, K., R. Sakthikumar and D. Sivakumar (2016). Interfacial oscillation of liquid jets discharging from non-circular orifices. *International Journal of Multiphase Flow* 87, 1–8.
- Rayleigh, L. (1879). On the capillary phenomena of jets. *Proc. R. Soc. London* 29, 71–97.
- Rayleigh, L. (1882). Xx. on the equilibrium of liquid conducting masses charged with electricity. The London, Edinburgh, and Dublin Philosophical Magazine and Journal of Science 14(87), 184–186.
- Reeder, M. F. and M. Samimy (1996, 03). The evolution of a jet with vortex-generating tabs: real-time visualization and quantitative measurements. *Journal of Fluid Mechanics* 311, 73–118.
- Reitz, R. and F. Bracco (1982). Mechanism of atomization of a liquid jet. *The Physics of Fluids* 25(10), 1730–1742.
- Schadow, K., K. Wilson, M. Lee and E. Gut- mark (1987). Enhancement of mixing in re-acting fuel-rich plumes issued from elliptical nozzles. *Journal of Propulsion and Power* 3, 145–149.
- Schneider, J., N. Lindblad, C. Hendricks Jr and J. Crowley (1967). Stability of an electrified liquid jet. *Journal of Applied Physics* 38(6), 2599–2605.
- Sharma, P. and T. Fang (2014). Breakup of liquid jets from non-circular orifices. *Experiments in fluids* 55(2), 1666.
- Sharma, P. and T. Fang (2015). Spray and atomization of a common rail fuel injector with non-circular orifices. *Fuel* 153, 416–430.
- Tabatabaee-Hosseini, P., B. Sadri and E. Esmaeilzadeh (2012). Experimental study on the impinging of two opposed inclined electrified laminar jets in the stagnant dielectric medium. *Experimental Thermal and Fluid Science* 42, 230 – 239.
- Tam, C. K. and D. E. Burton (1984). Sound generated by instability waves of supersonic flows. part 2. axisymmetric jets. *Journal of Fluid Mechanics* 138, 273–295.
- Taylor, G. (1969). Electrically driven jets. In *Proceedings of the Royal Society of London A: Mathematical, Physical and Engineering Sciences* 313, 453–475. The Royal Society.
- Wang, F. and T. Fang (2015). Liquid jet breakup for non-circular orifices under low pressures. *International Journal of Multiphase Flow* 72, 248–262.
- Weber, C. (1931). Zum zerfall eines flüssigkeitsstrahles. *ZAMM- Journal of Applied Mathematics and Mechanics/Zeitschrift für Angewandte Mathematik und Mechanik* 11(2), 136–154.
- Wlezien, R. and V. Kibens (1988). Influence of nozzle asymmetry on supersonic jets. *AIAA Journal* 26(1), 27–33.
- Zaman, K. B. M. Q., M. F. Reeder, and M. Samimy (1994). Control of an axisymmetric jet using vortex generators. *Physics of Fluids* 6(2), 778–793.